Probing nano-organization of astroglia with multi-color super-resolution microscopy

Janosch P Heller[1], Piotr Michaluk[1], Kohtaroh Sugao[1, 2] and Dmitri A Rusakov[1]

[1]: UCL Institute of Neurology, Department of Clinical and Experimental Epilepsy, Queen Square House, London WC1N 3BG, United Kingdom

[2]: Molecular Pathophysiology Research, Drug Research Division, Sumitomo Dainippon Pharma Co., Ltd.

Running title: Nanostructure of astroglia

Associate Editor: Special Issue on Brain Energy Metabolism

Key words: Astroglia, dSTORM, super-resolution microscopy, GFAP, S100β, glutamine synthetase, lck-GFP, pHluorin

Corresponding author: Dmitri Rusakov, UCL Institute of Neurology, Queen Square House, London WC1N 3BG, UK, E-mail: d.rusakov@ucl.ac.uk

Support: Wellcome Trust Principal Fellowship (101896), European Research Council Advanced Grant (323113-NETSIGNAL), FP7 ITN (606950 EXTRABRAIN), Russian Science Foundation grant (15-14-30000), Sumitomo Dainippon Pharma Co. (Tokyo).

ABSTRACT

Astroglia are essential for brain development, homeostasis and metabolic support. They also contribute actively to the formation and regulation of synaptic circuits, by successfully handling, integrating and propagating physiological signals of neural networks. The latter occurs mainly by engaging a versatile mechanism of internal Ca^{2+} fluctuations and regenerative waves prompting targeted release of signaling molecules into the extracellular space. Astroglia also show substantial structural plasticity associated with age- and use-dependent changes in neural circuitry. However, the underlying cellular mechanisms are poorly understood, mainly because of the extraordinary complex morphology of astroglial compartments on the nanoscopic scale. This complexity largely prevents direct experimental access to astroglial processes, most of which are beyond the diffraction limit of optical microscopy. Here we employed super-resolution microscopy (direct stochastic optical reconstruction microscopy; dSTORM), to visualize astroglial organization on the nanoscale, in culture and in thin bran slices, as an initial step to understand the structural basis of astrocytic nano-physiology. We were able to follow nanoscopic morphology of GFAP-enriched astrocytes, which adapt a flattened shape in culture and a sponge-like structure *in situ*, with GFAP fibers of varied diameters. We also visualized nanoscopic astrocytic processes using the ubiquitous cytosolic astrocyte marker proteins S100β and glutamine synthetase. Finally, we overexpressed and imaged membrane-targeted pHluorin and lymphocyte-specific protein tyrosine kinase-green fluorescent protein (lck-GFP), to better understand the molecular cascades underlying some common astroglia-targeted fluorescence imaging techniques. The results provide novel, albeit initial, insights into the cellular organization of astroglia on the nanoscale, paving the way for function-specific studies.

SIGNIFICANCE STATEMENT

Astroglia are a critical contributor to the development and function of brain circuits. However, the physiological basis of diverse astroglial activities remains largely an enigma, mainly because of the poor experimental access to the nanoscopic astroglial compartments filling the tissue volume. Super-resolution microscopy could thus provide an important tool to understand molecular organization of astrocytes on a small scale. Here we outline results of our initial quests to follow nano-organization of astroglial processes using super-resolution imaging of astroglia associated proteins GFAP, S100β and glutamine synthetase. These probes provide initial insights into the nano-organization of structurally intact astroglial on the scale from nanometers to microns, which has hitherto been unattainable.

INTRODUCTION

Astrocytes have emerged as an active neural circuit participant contributing to the information processing in the brain. They are equipped with numerous plasma membrane receptors, transporters and ion channels to enable receipt and transduction of diverse physiological inputs from the brain networks, in health and disease (reviewed in (Agulhon et al. 2008; Bennett et al. 2012; Dityatev and Rusakov 2011; Halassa and Haydon 2010; Haydon 2001; Matyash and Kettenmann 2010; Porter and McCarthy 1997; Seifert et al. 2010; Verkhratsky et al. 2012; Volterra and Meldolesi 2005)). Electrically non-excitable astroglia appear capable of integrating and communicating such physiological signals through the versatile machinery of intracellular calcium sparks, elevations and regenerative waves that exhibit wide-ranging spatiotemporal modalities across different cellular compartments (recently reviewed in (Araque et al. 2014; Bazargani and Attwell 2016; Khakh and Sofroniew 2015; Rusakov 2015; Volterra et al. 2014a; Zorec et al. 2012)). These Ca^{2+} fluctuations are translated by astrocytes into the release of signaling molecules, or gliotransmitters, - such as D-serine, glutamate, adenosine/ATP, α-TNC - triggering distinct functional responses in neurons (see references above).

This functional diversity coupled with the nearly universal Ca^{2+} dependence suggests that astroglia could operate specialized functional cellular compartments, on the microscopic or nanoscopic scale (Rusakov et al. 2014). In this context, much attention has been paid to ultrathin astrocyte processes that surround excitatory synapses (perisynaptic astrocytic processes, PAPs) and thus seem to provide a local cellular substrate for intimate astroglia-synapse signal exchange - most notably through glutamate transport and potassium buffering (Bergles et al. 1999; Danbolt 2001; Heller and Rusakov 2015; Rusakov et al. 2014) but also through the release of gliotransmitters. PAPs are present throughout the brain providing variable astroglial coverage of synapses depending on the region, the synaptic identity, but also on local circuit activity (Bernardinelli et al. 2014b; Haber et al. 2006; Heller and Rusakov 2015; Hirrlinger et al. 2004; Perez-Alvarez et al. 2014; Theodosis et al. 2008).

The cellular basis of versatile astroglial activity, and whether it involves specialized cellular compartments such as PAPs, remains poorly understood (recently reviewed by in (Bernardinelli et al. 2014a; Heller and Rusakov 2015)). This is mainly because direct experimental probing of the nanoscopic astrocyte structures has not been technically plausible: the sponge-like astrocyte processes fill the tissue volume featuring details that are beyond the diffraction limit of light microscopy (200-300 nm, including fluorescence confocal and two-photon excitation varieties). Historically, electron microscopy (EM) has been the only tool capable of successfully resolving astroglial

structure on the nanoscale, including advanced 3D reconstruction tools to deal with PAPs (Bernardinelli et al. 2014c; Lushnikova et al. 2009; Medvedev et al. 2014; Medvedev et al. 2010; Patrushev et al. 2013; Popov et al. 2004; Witcher et al. 2007; Witcher et al. 2010). However, EM has important limitations. Firstly, the extensive human and instrumental resources involved make it unfeasible to deal with more than a very few microscopic cell fragments in an individual 3D EM study. Correspondingly, obtaining a contiguous macroscopic pattern for the molecule of interest (receptor, channel, transporter, etc.) at nanoscopic resolution using EM will be technically challenging if at all feasible. In other words, EM has a limited ability to provide nanoscopic information in the context of the macroscopic organization of the cell and the surrounding tissue. Recent advances in super-resolution microscopy appear to overcome some of these deficiencies providing resolution of up to 10-70 nm while imaging structurally intact cells (Bates et al. 2007; Betzig et al. 2006; Huang et al. 2008; Klar et al. 2000). Applications of stimulated-emission depletion (STED), photo-activated localization microscopy (PALM) or stochastic optical reconstruction microscopy (STORM) are beginning to reveal some important aspects of astroglial nano-organization (Heller and Rusakov 2015; Panatier et al. 2014; Rossi et al. 2012; Smith and Verkman 2015; Volterra et al. 2014b).

Here, we adapt a direct STORM (dSTORM) technique, which uses stochastic excitation of sparsely distributed fluorophores (Endesfelder and Heilemann 2015; van de Linde et al. 2011), in an attempt to understand some basic aspects of the structural and molecular organization of astroglia on the nanoscale. We chose to image glial fibrillary acidic protein (GFAP), a common astroglia marker (Oberheim et al. 2012), a key astroglial metabolite glutamine synthetase (Derouiche and Frotscher 1991; Volterra et al. 2014b) and the calcium-binding protein S100β (Grosche et al. 2013; Nishiyama et al. 2002). We also overexpressed and imaged membrane-targeted pHluorin and lymphocyte-specific protein tyrosine kinase-green fluorescent protein (lck-GFP), to understand the expression nano-pattern of fusion proteins which represent a key tool in astroglia-targeted fluorescent imaging (Benediktsson et al. 2005; Endesfelder and Heilemann 2015; Shigetomi et al. 2010). Importantly, we probed these techniques in cultured astroglia (which tend to have a flattened, mainly two-dimensional morphology), in mixed cortical cultures (in which astroglia adopt a more sponge-like morphology) and also in thin brain sections that enable astrocyte structure imaging in three dimensions.

MATERIALS AND METHODS

Cortical cultures

All animal experiments in this study were carried out in full compliance with the corresponding UK and EU regulations. Cortical dissociated cultures from P0 rats were prepared as follows. We removed brains and isolated cortices on ice in Dissociation Medium (DM; 81.8 mM Na_2SO_4, 30 mM K_2SO_4, 5.8 mM $MgCl_2$, 0.25 mM $CaCl_2$, 1 mM HEPES, 20 mM glucose, 1 mM kynureic acid, 0.001% phenol red). Cortices we incubated in DM supplemented with 100 U Papain (Worthington, US-NY) twice for 15 minutes at 37°C; rinsed three times in DM and three times in plating medium (MEM, 10% FBS, 1% Penicilin/Streptomycin, 2mM GlutaMAX [Thermo Fisher Scientific]); triturated in plating medium until no clumps were visible. Cell solution was diluted 1:10 in OptiMEM (Thermo Fisher Scientific) and centrifuged at 1000 rpm for 10 minutes at room temperature. VCell pellet was re-suspended in plating medium, cells counted and plated at a density of 150,000 per 18 mm diameter coverslip (#1.5, scientific laboratory supplies) coated with 1 mg/ml poly-DL-lysine (Sigma) and 25 μg/ml laminin (Sigma). For mixed cortical cultures: three hours after plating medium was exchanged for maintenance medium (Neurobasal-A w/o Phenol Red, 2% B-27 Supplement, 1% Penicilin/Streptomycin, 0.5 mM GlutaMAX, 25 μM β-mercaptoethanol [Thermo Fisher Scientific]). For mixed cortical glial cultures: the next day plating medium was exchanged for glial medium (MEM 0.6% D-glucose, 1% Penicillin/Streptomycin, 10% horse serum 2mM L-glutamine), and cells were fed two to three times a week.

Transfection of cultured cells

Cells were transfected at 7 days *in vitro* (DIV) using Lipofectamine 3000 (Thermo Fisher Scientific) according to manufacturer instructions. Cells were incubated with Lipofectamine/DNA complexes in transfecting medium (MEM, 2% B-27 Supplement, 1 mM pyruvate, 0.5 mM GlutaMAX, 25 μM β-mercaptoethanol [Thermo Fisher Scientific]) for 1 hour at 37°C, 5% CO_2 in humidified incubator. After that cells were put back into their conditioned maintenance medium.

The plasmids that were used in this study were: pZac2.1gfaABC1D_Lck-GFP and pDisplay_SEP. pZac2.1gfaABC1D_Lck-GFP was created with standard cloning techniques based on the following plasmids: pZac2.1gfaABC1D_tdTomato (Addgene #44332, gift from Baljit Khakh (Shigetomi et al. 2013); pN1_Lck-GCaMP5G (Addgene #34924, gift from Baljit Khakh (Akerboom et al. 2012)); and a plasmid encoding GFP. pDisplay_SEP was created by cloning super-ecliptic pHluorin (SEP) into pDisplay_mSA-eGFP-TM (Addgene # 39863, gift from Sheldon Park (Lippman Bell et al. 2010)

Immunocytochemistry in culture

To perform super-resolution imaging of astrocytes in culture we labelled the cells using the following immunocytochemistry protocol (adapted from (Whelan and Bell 2015)). Pre-extraction was carried out using 0.2% saponin (Generon) in cytoskeleton-stabilization buffer (CSB; 10 mM MES pH 6.0, 138 mM KCl, 3 mM $MgCl_2$, 2 mM EGTA, 320 mM sucrose [Sigma]; warmed to 37°C) for 1 minute at room temperature. This was followed by: fixation with 3% formaldehyde (TAAB) + 0.1% glutaraldehyde (TAAB) diluted in CSB (warmed to 37°C) for 12-15 minutes at 37°C; washing with phosphate-buffered saline (PBS) twice for 2 and twice for 5 minutes gently rocking at room temperature; quenching with 0.1% $NaBH_4$ (Sigma) in PBS for 7 minutes gently rocking at room temperature; washing with PBS once for 2 and thrice for 5 minutes gently rocking at room temperature; permeabilization and blocking with blocking buffer (PBS supplemented with 0.1% saponin (PBS-S) and 3% bovine serum albumin (BSA, Sigma)) for 30 minutes gently rocking at room temperature. The samples were next incubated with primary antibodies (

Table 1) in PBS-S supplemented with 1% BSA overnight at 4°C; washed with PBS-S once for 2 and thrice for 10 minutes gently rocking at room temperature; incubated with fluorescently-labelled secondary antibodies (Table 2) diluted in PBS-S for one hour gently rocking at room temperature wrapped with aluminium foil; washed with PBS-S once for 10 minutes gently rocking at room temperature; incubated with fiducial markers (100 nm TetraSpeck microspheres, Thermo Fisher Scientific) diluted 1:500 in PBS for 20 minutes at room temperature, and washed with PBS-S once for 10 minutes and with PBS twice for 10 minutes at room temperature. Post fixation was carried out using 4% paraformaldehyde (PFA, Sigma) in PBS for 10 minutes at room temperature followed by washing with PBS thrice for 10 minutes gently rocking at room temperature, and samples were either imaged immediately or stored at 4°C. Seven DIV old mixed cortical glial cell cultures and 14 DIV old mixed cortical cultures were used for immunocytochemistry.

Immunohistochemistry in brain tissue sections

To perform super-resolution imaging of astrocytes in brain tissue sections we labelled the cells using the following immunocytochemistry protocol. Deeply anaesthetized rats (Sprague Dawley, 250 g) were perfused with ice-cold 4% PFA in PBS, brains were removed and incubated in 4% PFA in PBS overnight at 4°C, then sectioned using a vibratom (40 µm coronal sections). Sections were kept free-floating in PBS, incubated in 0.1% $NaBH_4$ in PBS for 15 min gently rocking at room temperature, then washed thrice for 5 min with PBS gently rocking at room temperature. Permeabilization and blocking were carried out using blocking buffer (PBS-S supplemented with 3% BSA) for 2 hours gently rocking at room temperature followed by incubation with primary antibodies in PBS-S (

Table 1) overnight gently rocking at 4°C. Samples were washed with PBS-S thrice for 10 minutes gently rocking at room temperature, incubated with fluorescently-labelled secondary antibodies (Table 2) diluted in PBS-S for two hours gently rocking at room temperature, washed with PBS-S twice for 10 minutes and with PBS thrice for 5 minutes gently rocking at room temperature. Post fixation was performed using 4% PFA in PBS for 30 minutes gently rocking at room temperature, followed by washing with PBS thrice for 10 minutes gently rocking at room temperature. Sections were incubated in Scale U2 buffer (4 M urea, 30% Glycerol and 0.1% Triton X-100 in water; Hama et al. 2011) and stored covered at 4°C until being prepared for imaging.

Table 1: Primary antibodies used.

ICC = Dilution factor used in immunocytochemistry, IHC = Dilution factor used in immunohistochemistry

Antigen	host	Clone	Supplier	product code	ICC	IHC
GFP	Chicken	polyclonal	Thermo	A10262	1:1000	N/A
GFP	Mouse	monoclonal	Merck	MAB3580	1:1000	N/A
GFAP	Mouse	GA5	Novus	NBP2-29415	1:1000	1:500
Glutamine synthetase	Mouse	monoclonal	abcam	ab64613	1:250	1:200
Glutamine synthetase	Mouse	GS6	Merck	MAB302	1:250	1:200
GFAP	Rabbit	Polyclonal	Novus	NB300-141	1:1000	1:500
S100β	Rabbit	Polyclonal	Synaptic systems	287 003	1:250	1:200

Table 2: Secondary antibodies used.

ICC = Dilution factor used in immunocytochemistry, IHC = Dilution factor used in immunohistochemistry

Antigen	Feature	Host	Supplier	product code	ICC	IHC
Chicken IgY	Alexa647-conjugated	Goat	Thermo	A21246	1:1000	N/A
Mouse IgG	CF568-conjugated	Donkey	Biotium	20105	1:500	1:200
Rabbit IgG	Alexa647-conjugated	Goat	Thermo	A21245	1:1000	1:500

Super-resolution imaging

Here, we employed the super-resolution imaging technique direct stochastic optical reconstruction microscopy (dSTORM) (Endesfelder and Heilemann 2015; van de Linde et al. 2011). Super-resolution images were recorded with a Vutara 350 commercial microscope (Bruker Corp., Billerica, US-MA) based on the single molecule localization (SML) biplane technology (Juette et al. 2008; Mlodzianoski et al. 2009). The targets were imaged using 647 nm (for Alexa647) and 561 nm (for CF568) excitation lasers, respectively, and a 405 nm activation laser in a photoswitching buffer containing 100 mM cysteamine and oxygen scavengers (glucose oxidase and catalase) (Metcalf et al. 2013). Images were recorded using a 60x-magnification, 1.2-NA water immersion

objective (Olympus) and a Flash 4.0 sCMOS camera (Hamatasu) with frame rate at 50 Hz. Total number of frames acquired per channel ranged from 5,000 to 20,000 frames. Data were analyzed using the Vutara SRX software (version 5.22). Single molecules were identified by their brightness frame by frame after removing the background. Identified particles were then localized in three dimensions by fitting the raw data with a 3D model function, which was obtained from recorded bead data sets. The experimentally achievable image resolution is 20 nm laterally (x and y) and 50 nm axially (z). With our methods we routinely achieve a lateral resolution of 38.2 ± 9.8 nm in cultured cells and 58.02 ± 7.09 nm in tissue sections and an axial resolution of 51.65 ± 20.61 nm in cultured cells and 73 ± 5.82 nm in tissue sections.

RESULTS

Nano localization of GFAP, S100β, and glutamate synthetase in mixed cortical glial cultures

First, we sought to image astrocytes in mixed cortical glial cultures. First, we employed the widely used astrocyte marker GFAP (Oberheim et al. 2012). Mixed cortical glial cells were cultured for one week in glial medium prior to fixation and immunostaining. Mouse or rabbit anti-GFAP antibodies were then labelled with secondary antibodies tagged with CF568 or Alexa647, which were used for dSTORM imaging. The images revealed a dotted structure of thin GFAP fibers forming a loose intracellular mesh (Figure 1). We next used a similar approach in an attempt to reveal the nanoscale distribution pattern of two other astroglia marker proteins that represent key cellular cascades and have been used extensively across the astroglial field, glutamine synthetase (Derouiche and Frotscher 1991; Volterra et al. 2014b) and the calcium-binding protein S100β (Grosche et al. 2013; Nishiyama et al. 2002). Again, mixed cortical glial cells were cultured for one week in glial medium prior to fixation and immunostaining. The images revealed spotty protein clusters, with the macroscopic pattern appearance drastically different form that of GFAP (Figure 2).

Nano localization of GFAP and S100β in mixed cortical cultures

Our next step was to visualize the expression patterns of all three marker proteins (GFAP, glutamine synthetase and S100β) in mixed cortical cultures, two weeks post-plating, using the methods similar to those in the previous section. We found that in the mixed cortical cultures, astrocytes showed a more sponge-like morphology, with several discernable GFAP-positive processes, in contrast to the more spread-out appearance in mixed glial cultures (Figure 3). Also in this culture the cells clearly expressed all the

astrocyte marker proteins under study. The super-resolution imaging revealed thin GFAP fibers that were virtually undetectable in the wide-field images (e.g., Figure 3I,S), in contrast to the dSTORM rendering (Figure 3J,T). Moreover, it appears as though glutamine synthetase and S100β fill out small astrocyte processes, the observation which has not hitherto been reported using conventional microscopy methods.

Nanoscopic imaging of the overexpressed pDisplay_SEP and pZac2.1gfaABC1D_Lck-GFP in astroglia in mixed cortical cultures

We next sought to explore the protein expression technique which has commonly been used to visualize fine astrocyte processes *in situ*: one week old mixed cortical cultures were transfected with either pDisplay_SEP or pZac2.1gfaABC1D_Lck-GFP using Lipofectamine 3000 (Thermo Fisher Scientific). This technique has been employed in the past to successfully visualize fine astrocyte processes *in situ* using conventional confocal or two-photon excitation microscopy (Benediktsson et al. 2005; Shigetomi et al. 2010). At 14 DIV the transfected cell cultures were used for immunostaining against GFP, to enable visualization the overall morphological outline of the cells under study. dSTORM imaging revealed ultra-thin astrocytic processes (below 100 nm in diameter) that were hardly detectable in the conventional wide-field images (Figure 4E and J). These observations indicated the feasibility of using the overexpression of membrane-targeted fluorescent proteins to resolve the nanostructure of ultrathin astrocytic processes that were beyond the diffraction limit of conventional optical microscopy.

dSTORM of GFAP expression in organized brain tissue

Thereafter, we set out to explore nanoscopic localization of GFAP in brain tissue sections. Fixed brains were sectioned (40 µm coronal sections) and used for immunohistochemistry (Materials and Methods). Once again, we labelled astrocytes using the common astrocytic marker GFAP (Oberheim et al. 2012). Similar to mixed cortical cultures, astrocytes *in situ* showed a sponge-like morphology, with several major GFAP-positive processes (Figure 5A-C). The GFAP fibers appear to be thicker in the proximity of the soma whereas in thin astrocyte processes they coudl only be identified reliably with super-resolution microscopy (Figure 5E).

Two-color dSTORM of glutamine synthetase and S100β in GFAP-labelled astroglia in situ

Finally, our objective was to obtain the nanoscale expression pattern and co-localization of glutamine synthetase and S100β in GFAP-expressing cells in brain tissue sections. As in the previous sections, fixed brains were cut into 40 µm coronal sections used for immunohistochemistry with respect to GFAP (Oberheim et al. 2012) (Figure 6A, K), glutamine synthetase (Derouiche and Frotscher 1991; Volterra et al. 2014b) (Figure 6D) and S100β (Grosche et al. 2013; Nishiyama et al. 2002) (Figure 6N). dSTORM enabled us to obtain intricate patterns of the three proteins in ultra-thin astroglial processes, the data not attainable with conventional microscopy (Figure 6J,T).

DISCUSSION

Nanoscopic astrocyte processes are omnipresent throughout the brain, shielding synapses to a varying degree and providing a platform for neurotransmitter uptake and gliotransmitters release (Bernardinelli et al. 2014b; Haber et al. 2006; Heller and Rusakov 2015; Hirrlinger et al. 2004; Perez-Alvarez et al. 2014; Theodosis et al. 2008). These processes are too small to be reliably detected by conventional microscopy. Therefore, EM has been the only tool used successfully to resolve glial structure on the nanoscale (Bernardinelli et al. 2014c; Lushnikova et al. 2009; Medvedev et al. 2014; Medvedev et al. 2010; Patrushev et al. 2013; Popov et al. 2004; Witcher et al. 2007; Witcher et al. 2010). Here, we documented first attempts to visualize thin astrocytic processes and their nano-organization using the super-resolution microscopy technique dSTORM. Using dSTORM we were able to reconstruct GFAP fibers in astrocytes *in vitro* as well as *in situ*. Moreover, we revealed the presence of glutamine synthetase and S100β in fine astrocytic protrusions, which were undetectable with widefield microscopy in culture and in brain sections. Lastly, we used overexpression of the membrane-targeted fluorescent proteins pHluorin and GFP to illuminate the entire outline of cultured astrocytes. Moreover, dSTORM revealed the presence of thin astrocytic processes that were not visible in conventional microscopy images. Taken together, this study provides evidence for the feasibility of dSTORM as a means to revealing thin astrocytic processes in cultured cells as well as in brain sections. Future experiments involving the analysis of the nano-organization of these processes will shed light on the intricate physiology of these cells protrusions.

Conflict of Interest Statement

The authors declare no conflict of interest.

Author contribution

Conception and design: JH and DR
Acquisition and analysis: JH, PM and KS
Drafting and revision of work: JH, PM and DR
Manuscript writing: JH and DR

Other Acknowledgments

The authors thank Drs Bao-Luen Chang and Andreas Lieb for providing rat brain tissue for sectioning.

REFERENCES

Agulhon C, Petravicz J, McMullen AB, Sweger EJ, Minton SK, Taves SR, Casper KB, Fiacco TA, McCarthy KD. 2008. What is the role of astrocyte calcium in neurophysiology? Neuron 59(6):932-946.

Akerboom J, Chen TW, Wardill TJ, Tian L, Marvin JS, Mutlu S, Calderon NC, Esposti F, Borghuis BG, Sun XR, Gordus A, Orger MB, Portugues R, Engert F, Macklin JJ, Filosa A, Aggarwal A, Kerr RA, Takagi R, Kracun S, Shigetomi E, Khakh BS, Baier H, Lagnado L, Wang SS, Bargmann CI, Kimmel BE, Jayaraman V, Svoboda K, Kim DS, Schreiter ER, Looger LL. 2012. Optimization of a GCaMP calcium indicator for neural activity imaging. J Neurosci 32(40):13819-13840.

Araque A, Carmignoto G, Haydon PG, Oliet SH, Robitaille R, Volterra A. 2014. Gliotransmitters travel in time and space. Neuron 81(4):728-739.

Bates M, Huang B, Dempsey GT, Zhuang X. 2007. Multicolor super-resolution imaging with photo-switchable fluorescent probes. Science 317(5845):1749-1753.

Bazargani N, Attwell D. 2016. Astrocyte calcium signaling: the third wave. Nat Neurosci 19(2):182-189.

Benediktsson AM, Schachtele SJ, Green SH, Dailey ME. 2005. Ballistic labeling and dynamic imaging of astrocytes in organotypic hippocampal slice cultures. Journal of neuroscience methods 141(1):41-53.

Bennett MV, Garre JM, Orellana JA, Bukauskas FF, Nedergaard M, Saez JC. 2012. Connexin and pannexin hemichannels in inflammatory responses of glia and neurons. Brain Res 1487:3-15.

Bergles DE, Diamond JS, Jahr CE. 1999. Clearance of glutamate inside the synapse and beyond. Curr Opin Neurobiol 9(3):293-298.

Bernardinelli Y, Muller D, Nikonenko I. 2014a. Astrocyte-synapse structural plasticity. Neural plasticity 2014:232105.

Bernardinelli Y, Randall J, Janett E, Nikonenko I, Konig S, Jones EV, Flores CE, Murai KK, Bochet CG, Holtmaat A, Muller D. 2014b. Activity-dependent structural plasticity of perisynaptic astrocytic domains promotes excitatory synapse stability. Current biology : CB 24(15):1679-1688.

Bernardinelli Y, Randall J, Janett E, Nikonenko I, Konig S, Jones EV, Flores CE, Murai KK, Bochet CG, Holtmaat A, Muller D. 2014c. Activity-dependent structural plasticity of perisynaptic astrocytic domains promotes excitatory synapse stability. Curr Biol 24(15):1679-1688.

Betzig E, Patterson GH, Sougrat R, Lindwasser OW, Olenych S, Bonifacino JS, Davidson MW, Lippincott-Schwartz J, Hess HF. 2006. Imaging intracellular fluorescent proteins at nanometer resolution. Science 313(5793):1642-1645.

Danbolt NC. 2001. Glutamate uptake. Progr Neurobiol 65:1-105.

Derouiche A, Frotscher M. 1991. Astroglial processes around identified glutamatergic synapses contain glutamine synthetase: evidence for transmitter degradation. Brain research 552(2):346-350.

Dityatev A, Rusakov DA. 2011. Molecular signals of plasticity at the tetrapartite synapse. Curr Opin Neurobiol 21(2):353-359.

Endesfelder U, Heilemann M. 2015. Direct stochastic optical reconstruction microscopy (dSTORM). Methods in molecular biology 1251:263-276.

Grosche A, Grosche J, Tackenberg M, Scheller D, Gerstner G, Gumprecht A, Pannicke T, Hirrlinger PG, Wilhelmsson U, Huttmann K, Hartig W, Steinhauser C, Pekny M, Reichenbach A. 2013. Versatile and simple approach to determine astrocyte territories in mouse neocortex and hippocampus. PloS one 8(7):e69143.

Haber M, Zhou L, Murai KK. 2006. Cooperative astrocyte and dendritic spine dynamics at hippocampal excitatory synapses. The Journal of neuroscience : the official journal of the Society for Neuroscience 26(35):8881-8891.

Halassa MM, Haydon PG. 2010. Integrated brain circuits: astrocytic networks modulate neuronal activity and behavior. Annu Rev Physiol 72:335-355.

Hama H, Kurokawa H, Kawano H, Ando R, Shimogori T, Noda H, Fukami K, Sakaue-Sawano A, Miyawaki A. 2011. Scale: a chemical approach for fluorescence imaging and reconstruction of transparent mouse brain. Nature neuroscience 14(11):1481-1488.

Haydon PG. 2001. GLIA: listening and talking to the synapse. Nat Rev Neurosci 2(3):185-193.

Heller JP, Rusakov DA. 2015. Morphological plasticity of astroglia: Understanding synaptic microenvironment. Glia.

Hirrlinger J, Hulsmann S, Kirchhoff F. 2004. Astroglial processes show spontaneous motility at active synaptic terminals in situ. The European journal of neuroscience 20(8):2235-2239.

Huang B, Wang W, Bates M, Zhuang X. 2008. Three-dimensional super-resolution imaging by stochastic optical reconstruction microscopy. Science 319(5864):810-813.

Juette MF, Gould TJ, Lessard MD, Mlodzianoski MJ, Nagpure BS, Bennett BT, Hess ST, Bewersdorf J. 2008. Three-dimensional sub-100 nm resolution fluorescence microscopy of thick samples. Nat Methods 5(6):527-529.

Khakh BS, Sofroniew MV. 2015. Diversity of astrocyte functions and phenotypes in neural circuits. Nat Neurosci 18(7):942-952.

Klar TA, Jakobs S, Dyba M, Egner A, Hell SW. 2000. Fluorescence microscopy with diffraction resolution barrier broken by stimulated emission. Proceedings of the National Academy of Sciences of the United States of America 97(15):8206-8210.

Lippman Bell JJ, Lordkipanidze T, Cobb N, Dunaevsky A. 2010. Bergmann glial ensheathment of dendritic spines regulates synapse number without affecting spine motility. Neuron glia biology 6(3):193-200.

Lushnikova I, Skibo G, Muller D, Nikonenko I. 2009. Synaptic potentiation induces increased glial coverage of excitatory synapses in CA1 hippocampus. Hippocampus 19(8):753-762.

Matyash V, Kettenmann H. 2010. Heterogeneity in astrocyte morphology and physiology. Brain Res Rev 63(1-2):2-10.

Medvedev N, Popov V, Henneberger C, Kraev I, Rusakov DA, Stewart MG. 2014. Glia selectively approach synapses on thin dendritic spines. Philos Trans R Soc Lond B Biol Sci 369(1654).

Medvedev NI, Popov VI, Rodriguez Arellano JJ, Dallerac G, Davies HA, Gabbott PL, Laroche S, Kraev IV, Doyere V, Stewart MG. 2010. The N-methyl-D-aspartate receptor antagonist CPP alters synapse and spine structure and impairs long-term potentiation and long-term depression induced morphological plasticity in dentate gyrus of the awake rat. Neurosci 165(4):1170-1181.

Metcalf DJ, Edwards R, Kumarswami N, Knight AE. 2013. Test samples for optimizing STORM super-resolution microscopy. J Vis Exp(79).

Mlodzianoski MJ, Juette MF, Beane GL, Bewersdorf J. 2009. Experimental characterization of 3D localization techniques for particle-tracking and super-resolution microscopy. Opt Express 17(10):8264-8277.

Nishiyama H, Knopfel T, Endo S, Itohara S. 2002. Glial protein S100B modulates long-term neuronal synaptic plasticity. Proceedings of the National Academy of Sciences of the United States of America 99(6):4037-4042.

Oberheim NA, Goldman SA, Nedergaard M. 2012. Heterogeneity of astrocytic form and function. Methods in molecular biology 814:23-45.

Panatier A, Arizono M, Nagerl UV. 2014. Dissecting tripartite synapses with STED microscopy. Philosophical transactions of the Royal Society of London Series B, Biological sciences 369(1654):20130597.

Patrushev I, Gavrilov N, Turlapov V, Semyanov A. 2013. Subcellular location of astrocytic calcium stores favors extrasynaptic neuron-astrocyte communication. Cell Calcium 54(5):343-349.

Perez-Alvarez A, Navarrete M, Covelo A, Martin ED, Araque A. 2014. Structural and functional plasticity of astrocyte processes and dendritic spine interactions. The Journal of neuroscience : the official journal of the Society for Neuroscience 34(38):12738-12744.

Popov VI, Davies HA, Rogachevsky VV, Patrushev IV, Errington ML, Gabbot PLA, Bliss TVP, Stewart MG. 2004. Remodelling of synaptic morphology but unchanged synaptic density during late phase long-term potentiation (LTP): A serial section electron micrograph study in the dentate gyrus in the anaesthetised rat. Neurosci 128(2):251-262.

Porter JT, McCarthy KD. 1997. Astrocytic neurotransmitter receptors in situ and in vivo. Prog Neurobiol 51(4):439-455.

Rossi A, Moritz TJ, Ratelade J, Verkman AS. 2012. Super-resolution imaging of aquaporin-4 orthogonal arrays of particles in cell membranes. J Cell Sci 125(Pt 18):4405-4412.

Rusakov DA. 2015. Disentangling calcium-driven astrocyte physiology. Nature Rev Neurosci 16(4):226-233.

Rusakov DA, Bard L, Stewart MG, Henneberger C. 2014. Diversity of astroglial functions alludes to subcellular specialisation. Trends Neurosci 37(4):228-242.

Seifert G, Carmignoto G, Steinhauser C. 2010. Astrocyte dysfunction in epilepsy. Brain Res Rev 63(1-2):212-221.

Shigetomi E, Bushong EA, Haustein MD, Tong X, Jackson-Weaver O, Kracun S, Xu J, Sofroniew MV, Ellisman MH, Khakh BS. 2013. Imaging calcium microdomains within entire astrocyte territories and endfeet with GCaMPs expressed using adeno-associated viruses. J Gen Physiol 141(5):633-647.

Shigetomi E, Kracun S, Khakh BS. 2010. Monitoring astrocyte calcium microdomains with improved membrane targeted GCaMP reporters. Neuron glia biology 6(3):183-191.

Smith AJ, Verkman AS. 2015. Superresolution Imaging of Aquaporin-4 Cluster Size in Antibody-Stained Paraffin Brain Sections. Biophysical journal 109(12):2511-2522.

Theodosis DT, Poulain DA, Oliet SH. 2008. Activity-dependent structural and functional plasticity of astrocyte-neuron interactions. Physiological reviews 88(3):983-1008.

van de Linde S, Loschberger A, Klein T, Heidbreder M, Wolter S, Heilemann M, Sauer M. 2011. Direct stochastic optical reconstruction microscopy with standard fluorescent probes. Nat Protoc 6(7):991-1009.

Verkhratsky A, Sofroniew MV, Messing A, deLanerolle NC, Rempe D, Rodriguez JJ, Nedergaard M. 2012. Neurological diseases as primary gliopathies: a reassessment of neurocentrism. ASN Neuro 4(3).

Volterra A, Liaudet N, Savtchouk I. 2014a. Astrocyte Ca^{2+} signalling: an unexpected complexity. Nat Rev Neurosci 15(5):327-335.

Volterra A, Liaudet N, Savtchouk I. 2014b. Astrocyte Ca(2)(+) signalling: an unexpected complexity. Nature reviews Neuroscience 15(5):327-335.

Volterra A, Meldolesi J. 2005. Astrocytes, from brain glue to communication elements: the revolution continues. Nature Rev Neurosci 6(8):626-640.

Whelan DR, Bell TD. 2015. Image artifacts in single molecule localization microscopy: why optimization of sample preparation protocols matters. Sci Rep 5:7924.

Witcher MR, Kirov SA, Harris KM. 2007. Plasticity of perisynaptic astroglia during synaptogenesis in the mature rat hippocampus. Glia 55(1):13-23.

Witcher MR, Park YD, Lee MR, Sharma S, Harris KM, Kirov SA. 2010. Three-dimensional relationships between perisynaptic astroglia and human hippocampal synapses. Glia 58(5):572-587.

Zorec R, Araque A, Carmignoto G, Haydon PG, Verkhratsky A, Parpura V. 2012. Astroglial excitability and gliotransmission: an appraisal of Ca2+ as a signalling route. ASN Neuro 4(2).

FIGURE LEGEND

Figure 1: dSTORM imaging of GFAP in astrocytes in mixed cortical glial cultures.

A: Wide-field image of astrocytes in mixed glial cultures expressing GFAP.

B: Area shown by rectangle in **A** at higher magnification, wide-field fluorescence mode.

C: Area as in **B** shown as a dSTORM image; GFAP fibers appear super-resolved, with single molecules making up the intermediate filament made discernible; blue clusters, fiducial markers used for drift correction. False color scale, focal depth.

D: Area shown by rectangle in **B** at higher magnification, wide-field fluorescence mode.

E: Area as in **B** shown as a dSTORM image; more detail and numerous individual GFAP fibers are visible at higher magnification.

F-J: Another example, notations and labelling are the same as in **A-E**.

Scale bars: A-C and F-H, 5 μm; D-E and I-J, 1 μm.

Figure 2: Nanoscopy of astrocytic marker proteins glutamine synthetase and S100β in mixed cortical glial cultures.

A: Wide-field image of astrocytes in mixed glial cultures expressing GFAP.

B: Area shown by rectangle in **A** at higher magnification, wide-field fluorescence mode.

C: A dSTORM image of area shown on **B**; individual molecules constituting the intermediate filament are visualized.

D: Wide-field image of glutamine synthetase (GS) in the same field of view as in A.

E: Area shown by rectangle in **D** at higher magnification, wide-field fluorescence mode.

F: A dSTORM image of area shown in E. Locations of individual glutamine synthetase molecules can be seen.

G: Merged image of B and E, with GFAP shown in green and GS in magenta, wide-filed fluorescence mode.

H: Merged image of F and H, with GFAP shown in green and GS in magenta, dSTORM.

I-J: Areas shown by rectangles in G and H, respectively. Individual GFAP fibers, as well as clusters of glutamine synthetase, are visible at higher magnification in the dSTORM image (J) while appearing undiscernible in wide-field mode (I).

K-T: A series of images, wide-field and dSTORM, illustrating expression pattern and nanoscopic co-localization of GFAP and S100β in mixed cortical glial cultures. GFAP is shown in green and S100β in magenta. Other notations are the same as in **A-J**.

Scale bars: A-H and K-R, 5 µm; I-J and S-T, 1 µm.

Figure 3: Comparison of GFAP, glutamine synthetase and S100β expression in mixed cortical cultures.

A-T: Wide-field and dSTORM images of astrocyte compartments in mixed cortical cultures, with the same notation and labelling as in Figure 2.

Scale bars: A-H and K-R, 5 µm; I-J and S-T, 1 µm.

Figure 4: Overexpression of membrane-targeted pHluorin or lck-GFP enables visualization of nanoscopic astrocytic processes.

A: Wide-field image highlighting the presence of pHluorin in transfected astroglia.

B: Area shown by a rectangle in **A** at higher magnification, wide-field fluorescence mode.

C: A dSTORM image of the area shown in **B**. Super-resolution image reveals the presence of distinct astrocytic domains that were unresolved with wide-field microscopy.

D and **E**: Areas shown by rectangles in **B and C**, respectively, at higher magnification in dSTORM mode. Image in E compared to the blown up wide-field images (D

F-J: Wide-field and dSTORM images of an astroglia transfected with and illuminated by lck-GFP; other notation and labelling are the same as in **A-E**.

Scale bars: A-C and F-H, 5 µm; D-E and I-J, 1 µm.

Figure 5: dSTORM imaging of GFAP in brain tissue sections.

A: An example of a wide-field image of GFAP-labelled astrocytes in brain sections.

B: Area shown by a rectangle in **A** at higher magnification, wide-field fluorescence mode.

C: A dSTORM image of area shown in **B**; GFAP fibers are resolved at the nanoscale, with individual discernable intermediate filaments.

D: Area shown by a rectangle in **B** at higher magnification, wide-field fluorescence mode.

E: Area shown by a rectangle in **C** at higher magnification, dSTORM.

Scale bars: A-C, 5 µm; D-E, 1 µm.

Figure 6: Nanoscopy of glutamine synthetase and S100β in GFAP-expressing cells in brain tissue sections.

A-T: Wide-field and dSTORM images of astrocyte compartments in brain tissue sections. Notation and labelling are the same as in Figure 2 and 3.

Scale bars: A-H and K-R, 5 μm; I-J and S-T, 1 μm.

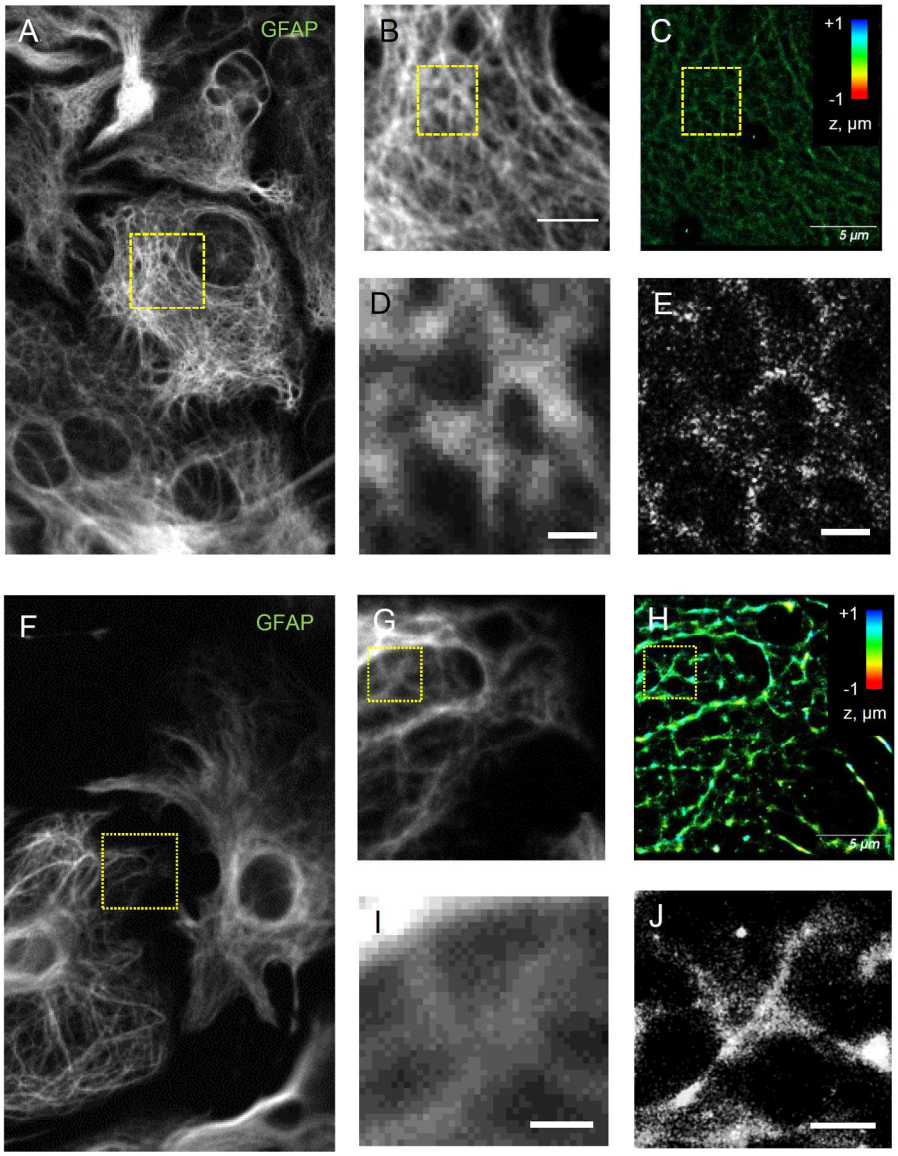

Figure 1

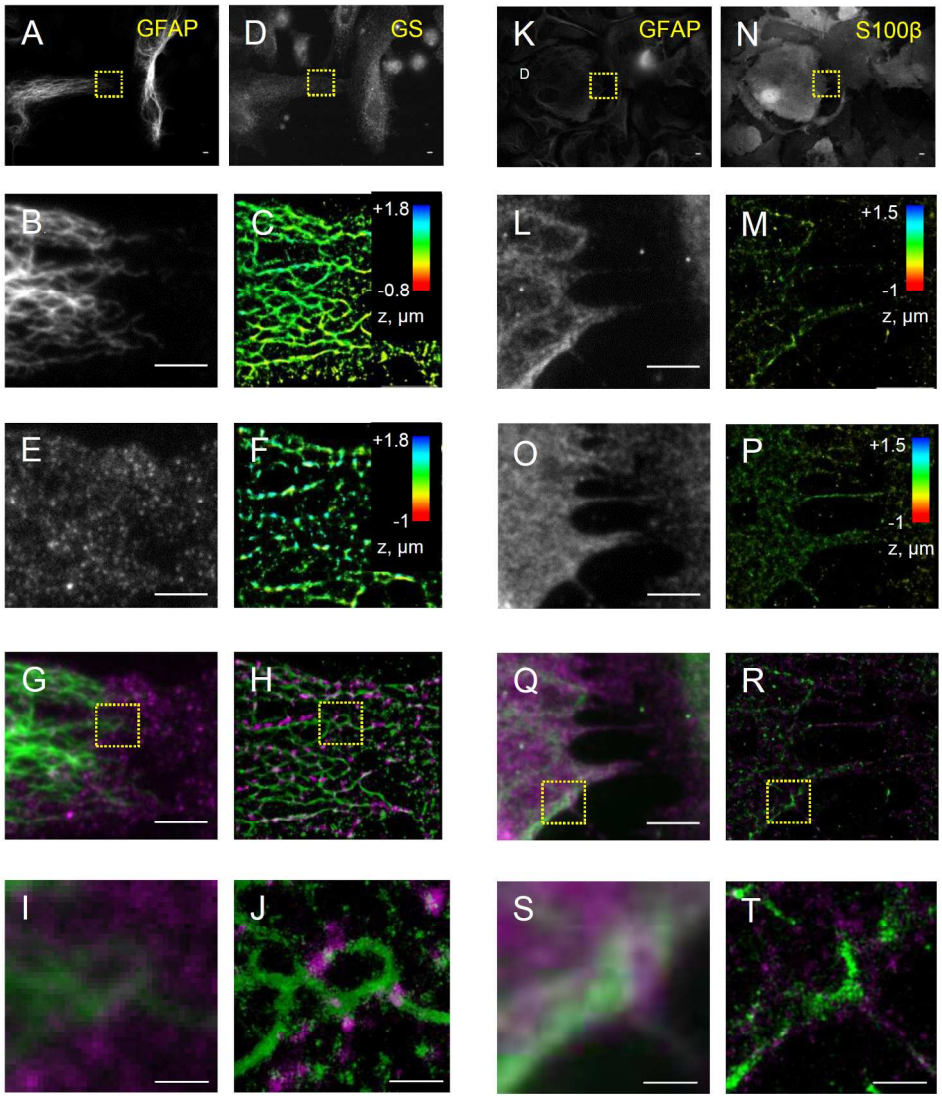
A
GFAP
D
GS
K
GFAP
D
N
S100β
B
C
+1.8
-0.8
z, μm
L
M
+1.5
-1
z, μm
E
F
+1.8
-1
z, μm
O
P
+1.5
-1
z, μm
G
H
Q
R
I
J
S
T

Figure 2

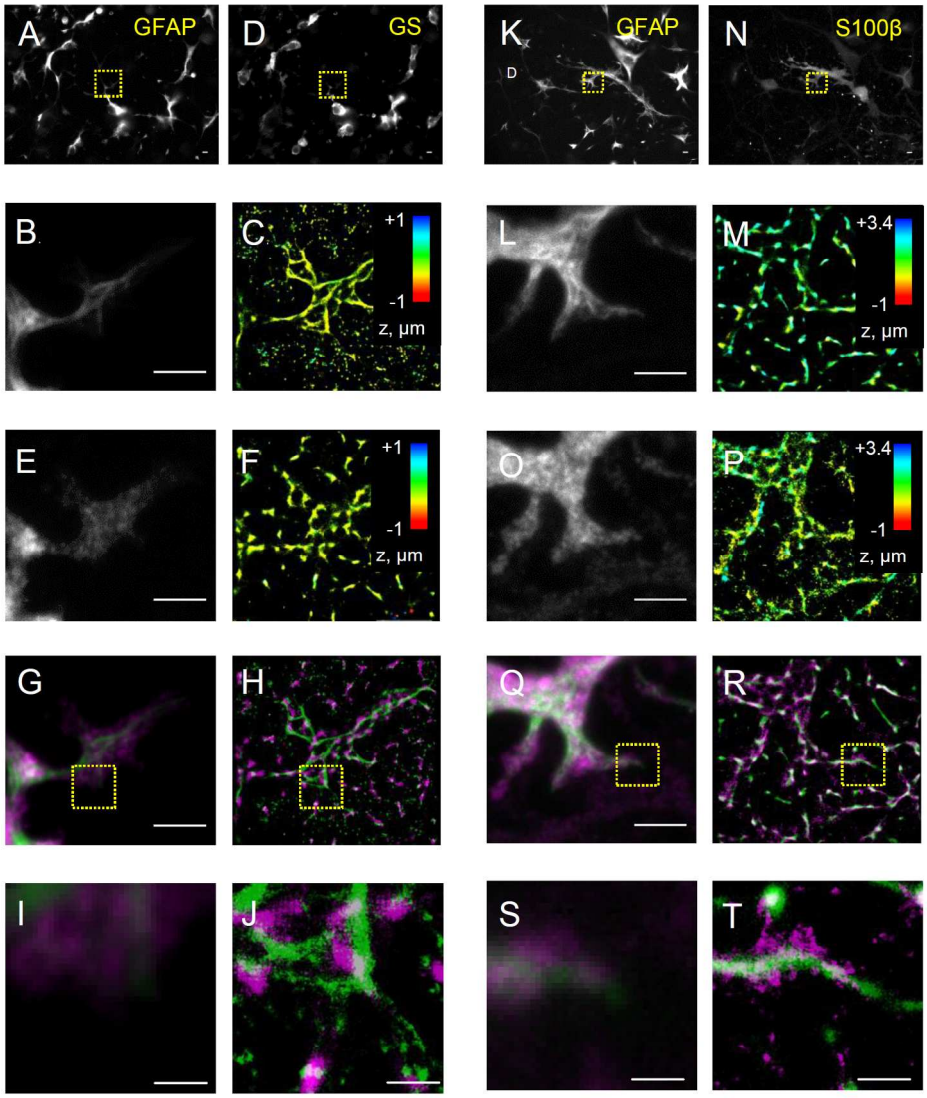
A
GFAP
D
GS
K
GFAP
D
N
S100β
B
C
+1
-1
z, μm
L
M
+3.4
-1
z, μm
E
F
+1
-1
z, μm
O
P
+3.4
-1
z, μm
G
H
Q
R
I
J
S
T

Figure 3

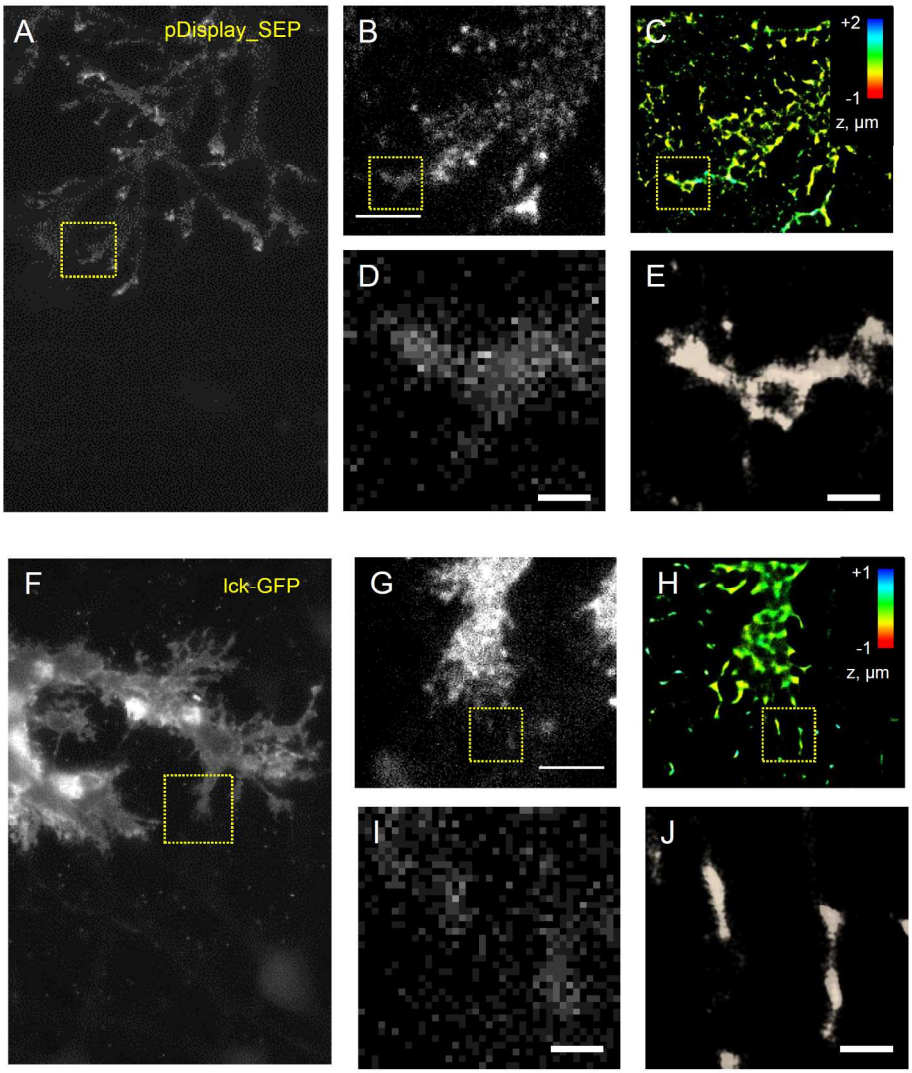

Figure 4

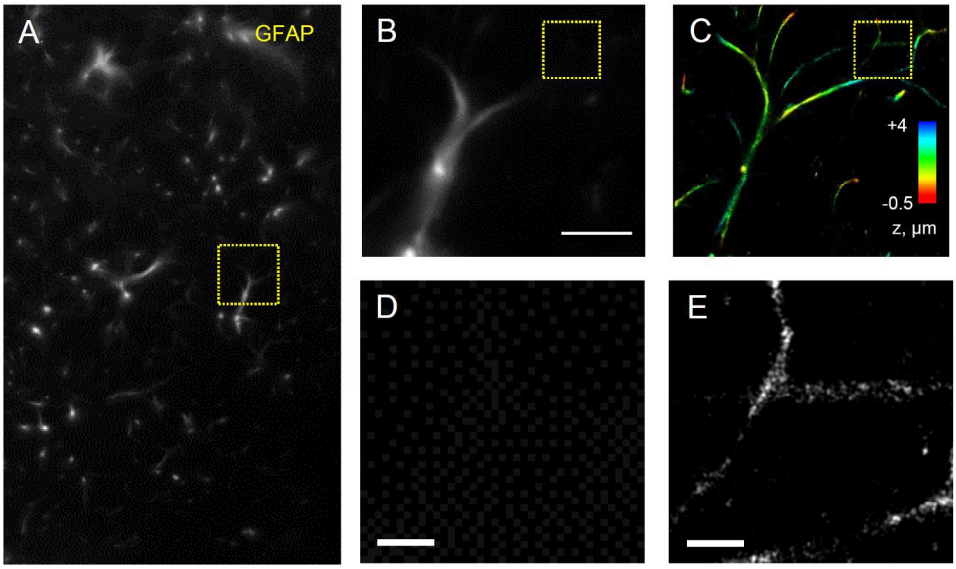

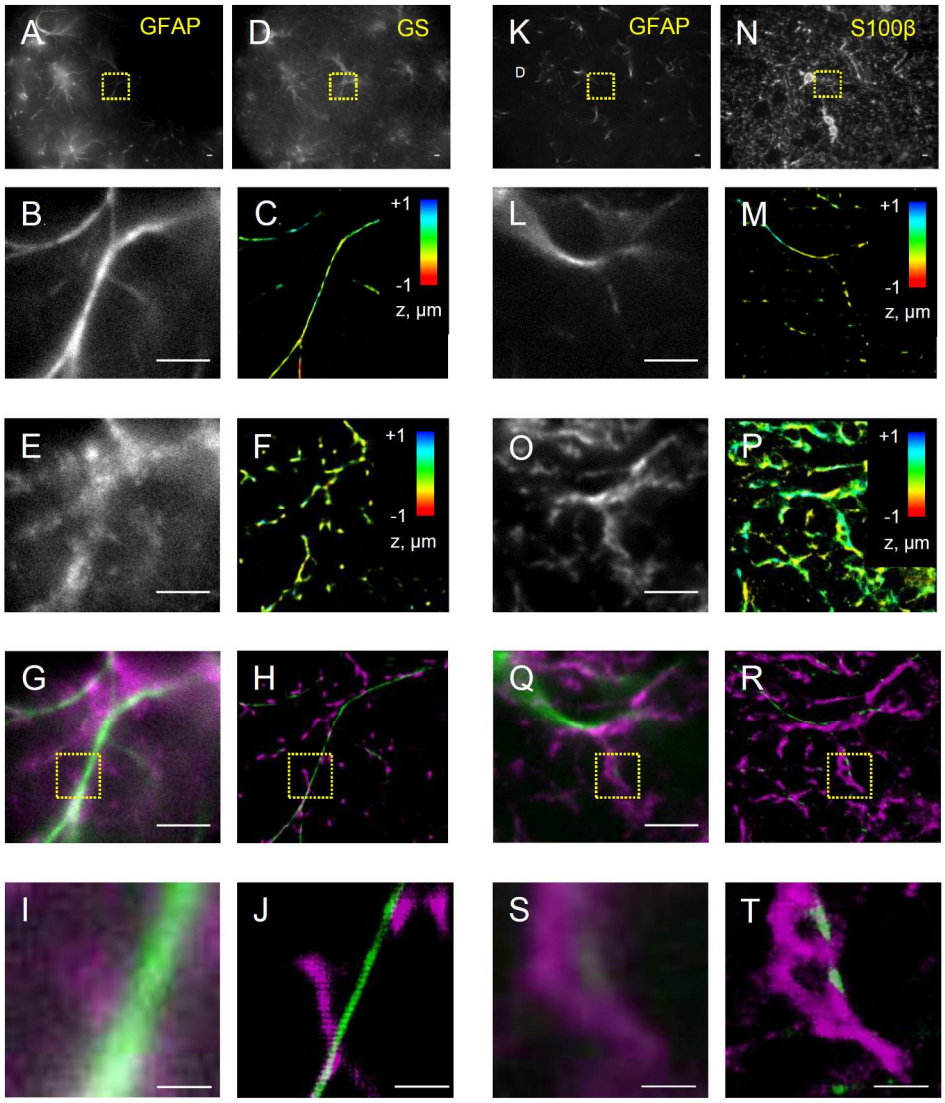
A
GFAP
D
GS
K
GFAP
D
N
S100β
B
C
+1
-1
z, μm
L
M
+1
-1
z, μm
E
F
+1
-1
z, μm
O
P
+1
-1
z, μm
G
H
Q
R
I
J
S
T

Figure 6